Journal of Power Sources 196 (2011) 5035–5044

Contents lists available at ScienceDirect

Journal of Power Sources

journal homepage: www.elsevier.com/locate/jpowsour

Novel fabrication technique of hollow fibre support for micro-tubular solid oxide fuel cells

Mohd Hafiz Dzarfan Othman [1], Nicolas Droushiotis, Zhentao Wu, Geoff Kelsall, K. Li *

Department of Chemical Engineering and Chemical Technology, Imperial College London, London SW7 2AZ, United Kingdom

ARTICLE INFO

Article history:
Received 4 October 2010
Received in revised form 19 January 2011
Accepted 2 February 2011
Available online 12 February 2011

Keywords:
Co-extrusion
Co-sintering
Dual-layer hollow fibre
Micro-tubular SOFC

ABSTRACT

In this work, a cerium-gadolinium oxide (CGO)/nickel (Ni)-CGO hollow fibre (HF) for micro-tubular solid oxide fuel cells (SOFCs), which consists of a fully gas-tight outer electrolyte layer supported on a porous inner composite anode layer, has been developed via a novel single-step co-extrusion/co-sintering technique, followed by an easy reduction process. After depositing a multi-layers cathode layer and applying current collectors on both anode and cathode, a micro-tubular SOFC is developed with the maximum power densities of 440–1000 W m^{-2} at 450–580 °C. Efforts have been made in enhancing the performance of the cell by reducing the co-sintering temperature and improving the cathode layer and current collection from inner (anode) wall. The improved cell produces maximum power densities of 3400–6800 W m^{-2} at 550–600 °C, almost fivefold higher than the previous cell. Further improvement has been carried out by reducing thickness of the electrolyte layer. Uniform and defect-free outer electrolyte layer as thin as 10 μm can be achieved when the extrusion rate of the outer layer is controlled. The highest power output of 11,100 W m^{-2} is obtained for the cell of 10 μm electrolyte layer at 600 °C. This result further highlights the potential of co-extrusion technique in producing high quality dual-layer HF support for micro-tubular SOFC.

1. Introduction

Micro-tubular solid oxide fuel cells (SOFCs) have received considerable attention in recent years due to the advantages of their design. The reduction in the size of SOFC leads to an increase in the volumetric power density as the power density scales with the reciprocal of the tube diameter [1]. Therefore, a 2 mm diameter micro-tubular SOFC could provide 10 times of more power per stack volume than a 20 mm diameter counterpart. Another order of magnitude increase could be achieved by further size reduction of the tube to 0.2 mm diameter, but this is difficult because the connections (e.g. current collection) are then more challenging and problematic to apply. Apart from enhancing power output of the fuel cell, high thermal shock resistance is also one of the major advantages of the micro-tubular design. Whereas the large-diameter tubular SOFC are prone to cracking if they are rapidly heated, the micro-tubular SOFCs do not crack even when heated in blow torch to their operating temperature of about 850 °C in as fast as 5 s [1]. Hence, this is a marked advantage in applications where start-up time is critical.

Previously, the fabrication of micro-tubular SOFC can only be achieved through multiple-step processes [2]. A support layer, for example anode-support, is first prepared to provide mechanical strength to the fuel cell, followed by deposition of electrolyte layer before a final cathode layer can be fabricated. Each step involves a high temperature heat treatment, making the cell fabrication extremely expensive. Clearly, combining the multiple steps into a single step is desirable in cutting production time and costs, and hence fuel cell price.

Phase inversion-based co-extrusion process is a promising technique to produce electrolyte/electrode dual-layer hollow fibre (HF) precursor for micro-tubular SOFC in a single step [3–6]. Prior to the co-extrusion process, the electrolyte and electrode (either anode or cathode) materials are separately mixed with solvent and polymer binder to form outer and inner layer suspensions, respectively. Both suspensions are then simultaneously co-extruded through a triple-orifice spinneret, passing through an air gap and finally into a non-solvent external coagulation bath. Concurrently, a stream of internal coagulant is supplied through the central bore of the spinneret. The layer thicknesses are controlled by the extrusion rate and sizes of the spinneret, while the macrostructure can be varied by adjusting suspension viscosity, air gap and flow rate of internal coagulant. The HF precursor is finally co-sintered at high temper-

* Corresponding author. Tel.: +44 (0) 207 5945676; fax: +44 (0) 207 5945629.
E-mail address: kang.li@imperial.ac.uk (K. Li).
[1] Present address: Advanced Membrane Technology Research Centre (AMTEC), Faculty of Petroleum and Renewable Energy Engineering, Universiti Teknologi Malaysia, 81310 Skudai, Johor, Malaysia.

0378-7753/$ – see front matter © 2011 Elsevier B.V. All rights reserved.
doi:10.1016/j.jpowsour.2011.02.006

Table 1
Compositions of the spinning suspension of first batch of dual-layer HFs.

Fibre name	Layer	Solvent type	Composition (wt.%)					Viscosity at 50 s^{-1} (cP)
			NiO	CGO	PESf	Arlacel P135	Solvent	
HF1	Anode	NMP	39.60	26.40	6.60	0.12	27.28	6690
	Electrolyte		–	64.00	6.40	0.12	29.48	8490
HF2	Anode	NMP	40.80	27.20	6.80	0.12	25.08	7150
	Electrolyte		–	64.00	6.40	0.12	29.48	8490
HF3	Anode	NMP	42.60	28.40	7.10	0.12	21.78	24,400
	Electrolyte		–	64.00	6.40	0.12	29.48	8490
HF4	Anode	DMSO	42.00	28.00	7.00	0.12	22.88	32,500
	Electrolyte		–	64.00	6.40	0.12	29.48	14,900

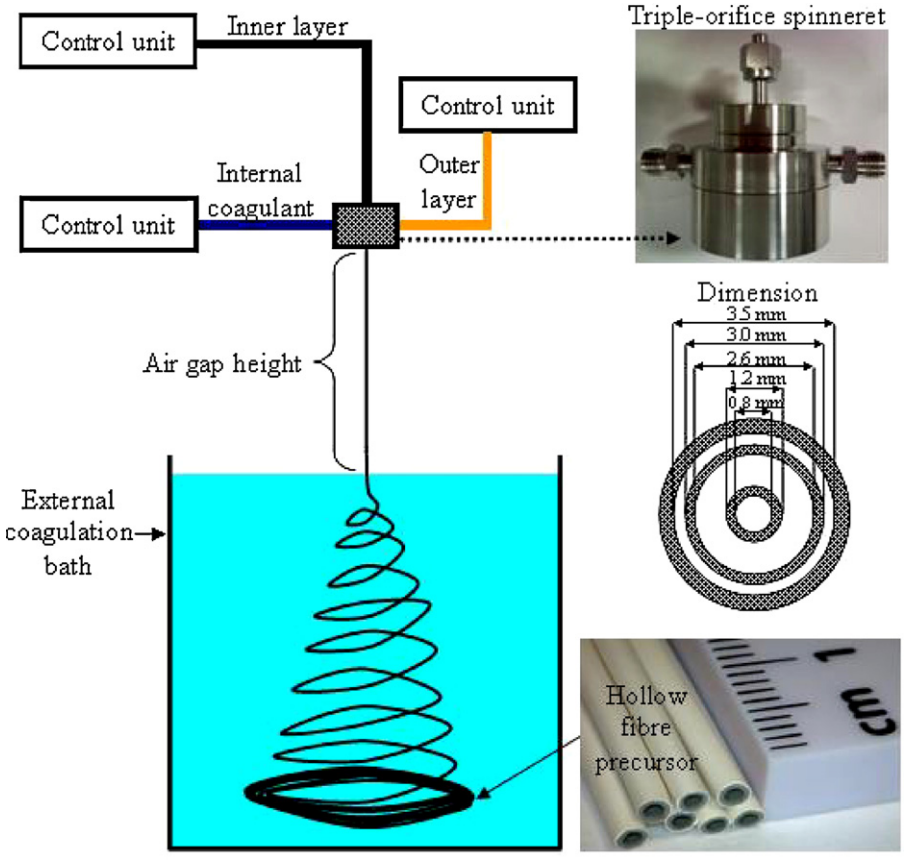

Fig. 1. Schematic diagram of phase inversion-based co-extrusion process.

ature as a procedure to remove polymer binder and densify the ceramic materials.

This paper reports about the fabrication of cerium-gadolinium oxide (CGO)/nickel oxide (NiO)-CGO dual-layer HF using novel co-extrusion process. In the early stage of this work, four HFs with variation in the anode structures were prepared. However, only HF with asymmetric structure was chosen to be characterised. The HF was co-sintered at temperature of 1550 °C and then followed by a simple reduction process. A number of improvements, such as on the co-sintering temperature, cathode deposition technique, current collection method and electrolyte layer thickness, have also been carried out to optimize the performance of the cell and will be discussed in detail in this paper.

Table 2
Co-extrusion conditions of the HF1, HF2 and HF3.

Fibre name	Layer	Extrusion pressure (psig)	Flow rate of internal coagulant (cm^3 min^{-1})	Air gap (cm)
HF1	Anode	15		
	Electrolyte	20		
HF2	Anode	15	13	15
	Electrolyte	20		
HF3	Anode	15		
	Electrolyte	20		

Table 3
Co-extrusion conditions of the HF4.

Fibre name	Layer	Extrusion rate (cm^3 min^{-1})	Flow rate of internal coagulant (cm^3 min^{-1})	Air gap (cm)
HF4	Anode	7	10	20
	Electrolyte	7		

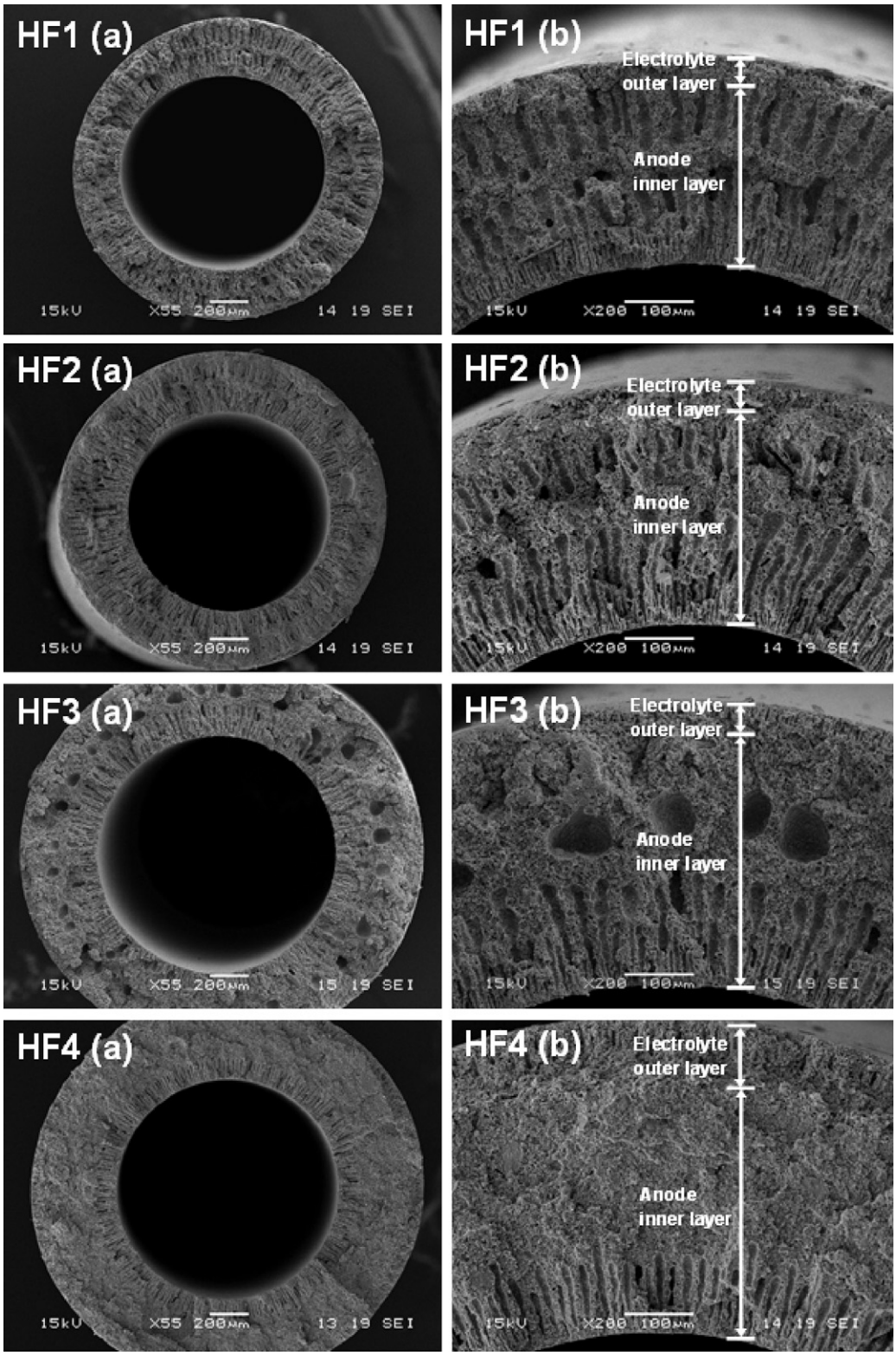

Fig. 2. SEM images of the (a) overall view and (b) cross-section of the CGO/NiO–CGO dual-layer HF precursors of HF1, HF2, HF3 and HF4.

2. Materials and experimental methods

2.1. Materials

Commercially available cerium-gadolinium oxide ($Ce_{0.9}Gd_{0.1}O_{1.95}$ or CGO, surface area 35 $m^2\,g^{-1}$ d_{50} 0.32 μm) and nickel oxide (NiO, surface area 5 $m^2\,g^{-1}$ d_{50} 0.55 μm) were purchased from NexTech Materials Ltd. (Ohio) and were used as supplied. Polyethersulfone (PESf) (Radel A-300, Ameco Performance, USA), N-methyl-2-pyrrolidone (NMP) (HPLC grade, Rathbone) or dimethyl sulfoxide (DMSO) (Sigma–Aldrich), and polyethyleneglycol 30-dipolyhydroxystearate (Arlacel P135, Uniqema) were used as a polymer binder, solvent, and additive, respectively. Tap water and de-ionized water were

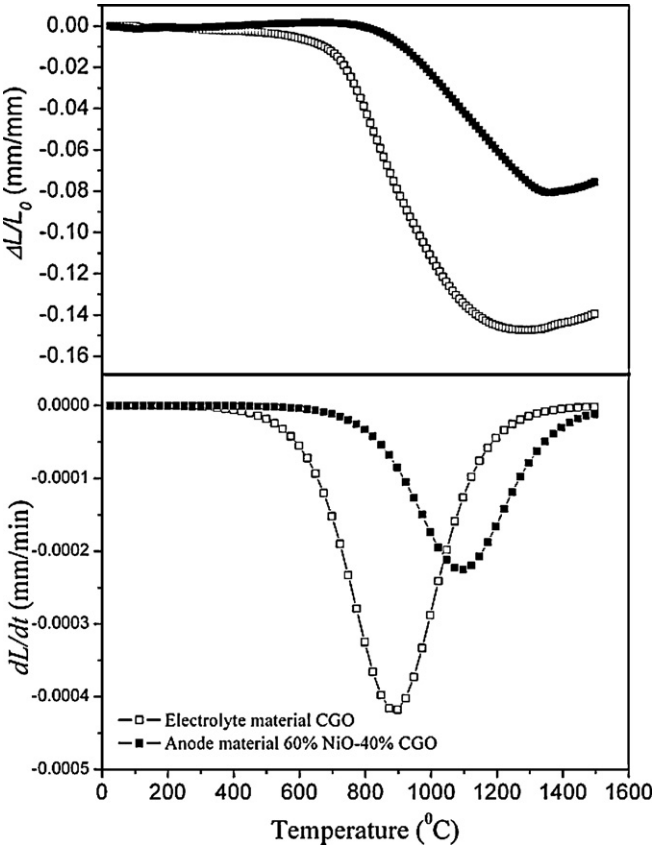

Fig. 3. (a) Sintering curves and (b) sintering rate curves of the inner and outer layer materials (heating rate 3 °C min^{-1}).

used as the external and internal coagulants, respectively. Lanthanum strontium cobalt ferrite, $La_{0.6}Sr_{0.4}Co_{0.2}Fe_{0.8}O_3$ (LSCF) (NexTech Materials Ltd., Ohio) and ethylene glycol (99+%, Acros Organic) were used as the materials for cathode slurry.

2.2. Preparation of electrolyte/anode dual-layer HFs

The detail about the fabrication of dual-layer HFs has been described elsewhere [4]. In the preparation of the electrolyte/anode dual-layer HFs, two ceramic suspensions were prepared separately. The suspension of the anode inner layer was composed of 60 wt.% of NiO and 40 wt.% of CGO, while the one for the electrolyte outer layer contained CGO powder only. The suspensions compositions of four different dual-layer HFs are listed in Table 1, in which the fibres are named as HF1, HF2, HF3 and HF4 according to the weight percentages of ceramic powders in the suspensions. Ceramic powders were first mixed with solvent (i.e. NMP or DMSO) and additive and stirred for 48 h, after which PESf pellets were slowly added into the mixtures under stirrer (OST 20 Digital YELLOWLINE IKA) rotation speed at ~300 rpm. The mixing was further carried out for an extra 48 h to obtain homogeneous spinning suspension.

The dual-layer HF precursors were prepared by a phase inversion-based co-extrusion process. Prior to the co-extrusion, both spinning suspensions were degassed at room temperature under stirring to fully remove the air trapped inside the suspensions. The both spinning suspensions were then loaded into a stainless steel container and co-extruded through a triple orifice spinneret, which schematically illustrated in Fig. 1. The inner and outer layer spinning suspensions of HF1, HF2 and HF3 were pressurized using nitrogen gas, where the procedure has been described in detail elsewhere [7], while the extrusion rate of inner and outer layers for HF4 were accurately monitored and controlled by syringe pumps (PHD 2000 Programmable, HARVARD APPARATUS). The operating conditions employed for preparing the electrolyte/anode dual-layer HFs are summarized in Tables 2 and 3.

The selected dual-layer HF precursors were then co-sintered in a tube furnace (TSH17/75/450, ELITE) under static air atmosphere. The temperature was increased from room temperature to 400 °C at a rate of 2 °C min^{-1} and held for 1 h, then to 800 °C at a rate of 2 °C min^{-1} and held for 2 h and finally to target temperatures (i.e. 1550 and 1500 °C) at a rate of 15 °C min^{-1} and held for 12 h. The temperature was then reduced to room temperature at a rate of 5 °C min^{-1}. Finally, the co-sintered CGO/NiO-CGO HFs were reduced to CGO/Ni-CGO HFs in a tube reactor using pure hydrogen. The tube was inserted into a horizontal furnace (MTF 12/25/250, CARBOLITE). Argon of 30 cm^3 min^{-1} (20 °C, 1 atm) was used to expel the air until the reactor temperature reaches 550 °C, following which the argon flow was replaced by pure hydrogen of 20 cm^3 min^{-1} (20 °C, 1 atm). After 2.5 h of reduction, the flow of hydrogen was switched to argon until the temperature was reduced to room temperature. The heating and cooling rates were kept at 4 °C min^{-1}.

2.3. Characterizations of dual-layer HFs

Viscosities of the suspensions were tested by Physica UDS-200 rheometer using concentric cylinder geometry at 20 °C. Spinning suspension samples were taken and tested immediately prior to fibre spinning. The morphology of the dual-layer HFs was examined using a JEOL JSM-5610 scanning electron microscope (SEM). The HFs were snapped in order to obtain cross-sectional fracture. These HF samples were then placed on a metal holder and sputtered by gold under vacuum. High resolution images of the cross-section of the HFs were taken at different magnifications using secondary electron imaging (SEI) and backscattered electrons (BSE) modes. The sintering behaviours of the inner and outer layers' materials were studied using dilatometer (Netzsch, model DIL 402C). After mixing in ethanol, the mixtures of powders were pressed into rectangular bars with the dimensions of 6 mm × 6 mm × 20 mm for testing. The measurements were carried out under static air atmosphere, using a heating rate of 3 °C min^{-1} from room temperature to 1500 °C. The elemental distribution at the interface between inner and outer layers of the HF was analyzed by energy dispersive X-ray spectroscopy (EDS) technique using JEOL 840 SEM.

X-ray diffraction (XRD) was used to identify the crystal phases of inner and outer layers of the developed HF and to investigate the reduction of NiO. XRD analysis was applied using an x'celerator detector, soller 004 rad (X'Pert PRO model) and a Cu X-ray tube with Kα radiation (λ = 154.2 pm). The sintered samples were analyzed in the range of $10 \leq 2\theta(^\circ) \leq 80$ at a 1° scan rate.

3. Results and discussion

3.1. Macrostructure

Apart from showing schematically the co-extrusion process, Fig. 1 also shows a photographic image of the dual-layer HF precursors developed in this study. The light yellow precursor contains CGO powder and PESf polymer in the outer layer, and a dark green mixture of NiO-CGO powders and PESf in the inner layer. As can be seen in Fig. 2, anode inner layer cross-section of HF1 exhibits a sandwich-like structure with finger-like voids from both inner and outer sides, leaving a small sponge-like structure in the middle of the HF. It is believed that only finger-like voids from inner surface

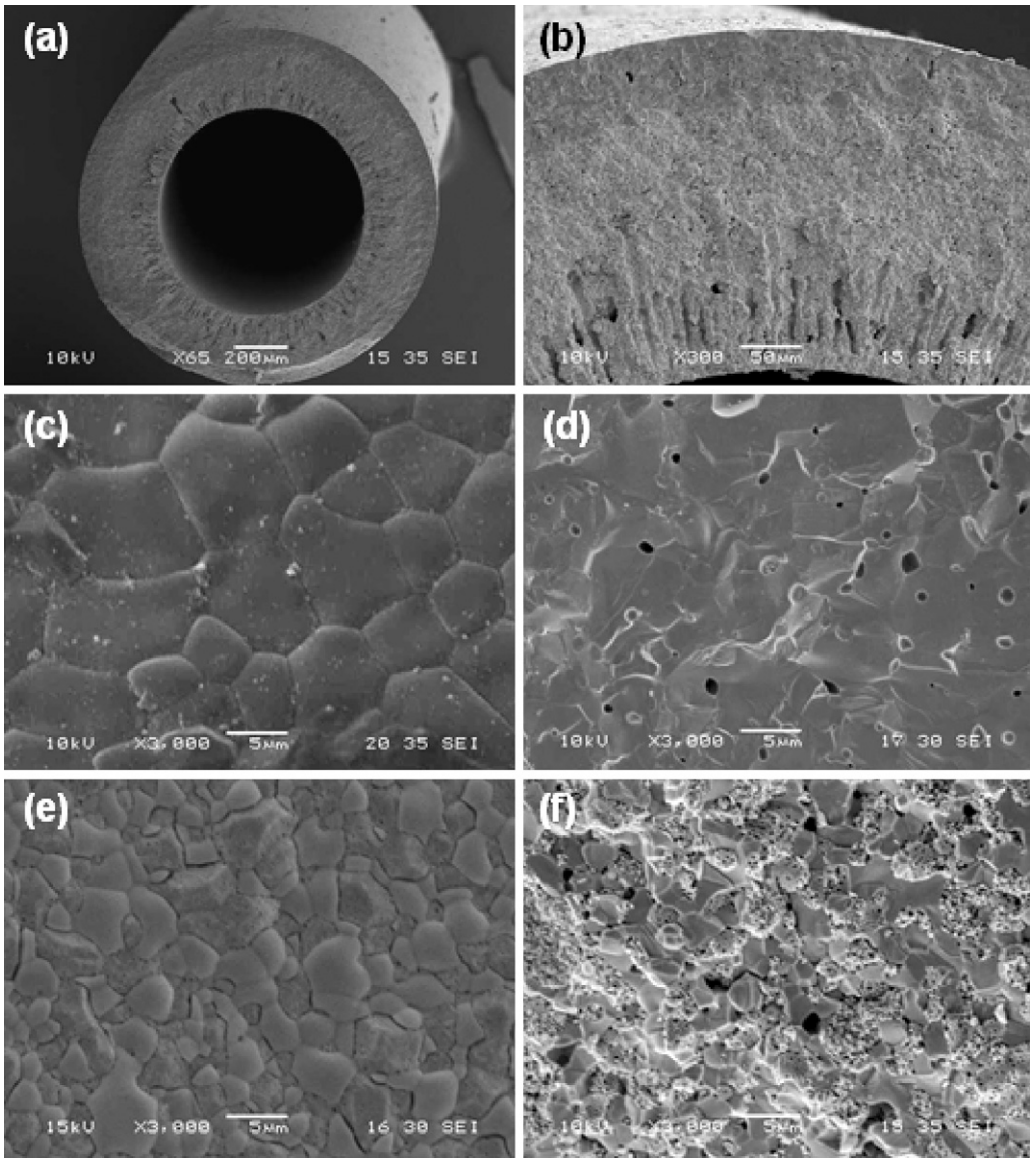

Fig. 4. SEM images of different skins of the HF4 co-sintered at 1550 °C; (a) overall view of the HF, (b) cross-section of the HF, (c) outer surface of the HF, (d) electrolyte cross-section of the HF, (e) inner surface of the HF and (f) anode cross-section of the HF.

could facilitate the fuel transport in the anode, while the presence of the voids from outer side would reduce the conductivity and mechanical strength of the HF and affect the gas-tightness property of the electrolyte outer layer. Therefore, effort has been made to eliminate the finger-like voids created from the outer surface of the anode by increasing the initial viscosity of the inner layer suspension. Kingsbury and Li [8] described in their research that the finger-like voids are formed when the suspension comes in contact with the coagulant, which results in solvent/coagulant exchange, leading to a rapid increase in local viscosity and finally precipitation of the polymer binder phase. However, due to instabilities at the interface between the suspension and the coagulant, there is a tendency for viscous fingering to occur, initiating the formation of finger-like voids. Above a critical level of suspension viscosity, this phenomenon is not observed and a sponge-like structure is formed.

As can be seen in Table 1, the inner layer suspension viscosity is increased by the increase of particles (mixed NiO and CGO) loading from 66 wt.% to 68 wt.%, and is dramatically enhanced when the particles loading is 71%. Although the fibre HF2 prepared from 68 wt.% has similar structure with HF1, in which the finger-like voids are created from both inner and outer anode sides, the void length and size from the outer side of anode have been reduced. A sponge-like region occupying approximately 20% of the fibre cross-section presents between the inner and outer finger-like voids. The thickness of the finger-like voids structure is further reduced when the particles loading is increased to 71 wt.%, as shown in SEM images for HF3. However, the macro-voids structure from the outer surface of anode in HF3 is still created due to the insufficient viscosity to prevent the formation of such void structure.

Therefore, dimethyl sulfoxide (DMSO) is introduced as a solvent to replace NMP in order to further suppress the formation of finger-like voids in outer surface of the inner layer. DMSO was chosen due to its high freezing point (i.e. 18.5 °C), which increases the initial suspension viscosity and results in an incipient increase of the resistance against the formation of finger-like voids (i.e. freezing effect) [9]. As a result, different morphology is formed for HF4 as it presents an asymmetric structure with short finger-like voids structures originating from the inner surface to approximately 35% of the inner layer thickness, whereas the other 65% consists of a sponge-like structure.

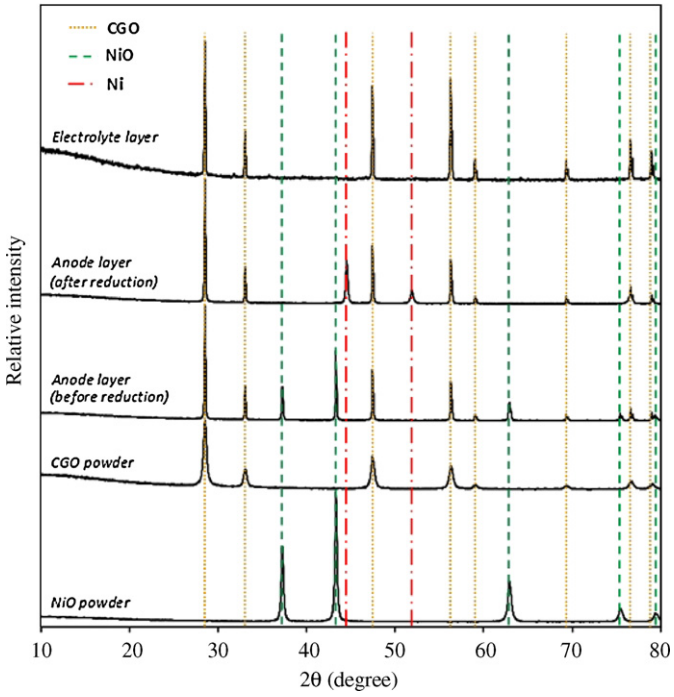

Fig. 5. XRD patterns of the anode inner layer and electrolyte outer layer of the dual-layer HF.

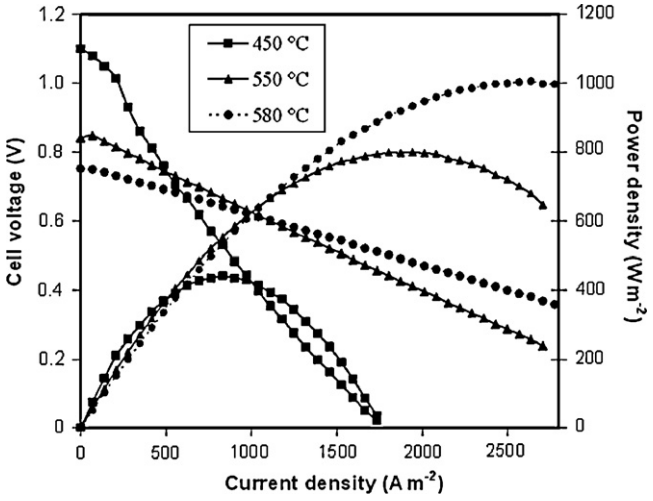

Fig. 6. Voltages and power densities as functions of current density for the cell of HF4.

As can also be observed in Fig. 2, the electrolyte outer layer for all dual-layer HF is uniformly deposited on the anode inner layer and there is very good adhesion between the outer and inner layers. The electrolyte outer layers of the HF1, HF2 and HF3 have similar thickness due to the use of same suspension composition and co-extrusion conditions, however HF4 which used DMSO as a solvent shows a thicker electrolyte layer. The outer layer of HF4 also shows small finger-like voids near the outer surface and sponge-like structures occupying the rest of the layer.

Due to the desire anode structure achieved for HF4, only HF4 was co-sintered, reduced and characterized. For ceramic membranes with a dual-layer structure, especially made of different materials, co-sintering is always challenging due to the different sintering behaviours of the membrane materials. The co-sintering of ceramic HFs would be more difficult because of higher surface area and higher curvity of the HFs when compared with disk or tubular counterparts. Before the co-sintering of the dual-layer HF, the sintering behaviours of the HF materials were investigated, the results of which are shown in Fig. 3. When compared with the inner anode layer, the outer electrolyte layer starts to shrink at lower temperature with a much higher final shrinkage of about 14.7% (Fig. 3(a)). Moreover, the highest sintering rate of the outer layer is almost twice of that of the inner layer and turns up at a temperature of about 200 °C lower that of the inner layer. Due to the significantly different sintering behaviours between inner and outer layers, as shown in Fig. 3, a heating rate as high as 15 °C min^{-1} has to be used during the co-sintering process, below which heating rate, the fibres might not survive the co-sintering, as has been observed experimentally.

After co-sintering the CGO/NiO-CGO precursor fibres of HF4 at 1550 °C for 12 h and reducing NiO in the inner layer to Ni, a CGO/Ni-CGO dual-layer HF for micro tubular SOFC was obtained. The macrostructure of the resultant CGO/Ni-CGO dual-layer HF are shown in Fig. 4(a) and (b). The outer diameter (OD) and the inner diameter (ID) of the dual-layer HF were measured to be of approximately 1400 and 800 μm, and the thicknesses of the inner and the outer layer are ca. 220 μm and 80 μm. The SEM images of the electrolyte layer in Fig. 4(c) and (d) show that the electrolyte layer has a dense structure, as required for it to be gas-tight, preventing direct contact between fuel and oxidant. It can also be seen from Fig. 4(e) and (f) that the general surface and cross-sectional structures of the anode inner layer, respectively, is largely retained after co-sintering and reduction processes, where all of them still have distinguished morphologies as described for the HF precursor. This suggests that the co-sintering and reduction processes do not cause any major changes in anode macrostructure. Although the densification of HF occurs in co-sintering process and would reduce the porosity, the removal of oxygen atoms from NiO by hydrogen during the reduction process allows the structure of the fibre to be more porous, especially in the sponge-like region.

In Fig. 5, X-ray diffraction (XRD) patterns of the anode inner layer (before and after reduction) are compared with the original CGO and NiO powders. As can be seen, no secondary phase is found besides cubic phases of NiO and CGO in the anode after the co-sintering. Furthermore, NiO was fully reduced into Ni at 550 °C using hydrogen, without affecting the structure of CGO. All these are in agreement with Chen's work [10]. The outer surface of the electrolyte layer was also characterized by XRD, and no Ni or NiO phase is detected. This indicates that, during the co-sintering process, there is no inter-diffusion between the layers.

3.2. Electrochemical performance of the micro-tubular SOFCs co-sintered at 1550 °C

Prior to the electrochemical measurements, multi-layers of cathode materials (i.e. 2 layers of CGO-LSCF cermet and 1 layer LSCF) were deposited on the electrolyte of the dual-layer HFs by brush painting technique and sintered at 970 °C for 2 h to form a 10 mm length cathode. Silver wire was then wrapped around the 10 mm long cathode and conductive silver paste was used to improve the connection of the wire to the cathode surface. Another silver spiral wire was inserted inside the fibre lumen to collect the current from the anode. The resultant micro-tubular SOFC was fixed in a gas-tight aluminium tube using a cement sealing paste after applying current collectors. The size of the cell was about 1.5 mm in diameter with the active cathode length of 10 mm. Prior to the fuel cell test, the anode of the cell was pre-conditioned in 5 cm^3 min^{-1} of hydrogen (saturated with water vapour of 0.12 cm^3 min^{-1} at 20 °C, 1 atm) at 550 °C for 2.5 h, in order to achieve complete conversion of NiO-CGO to Ni-CGO. Hydrogen of 15 cm^3 min^{-1} (saturated

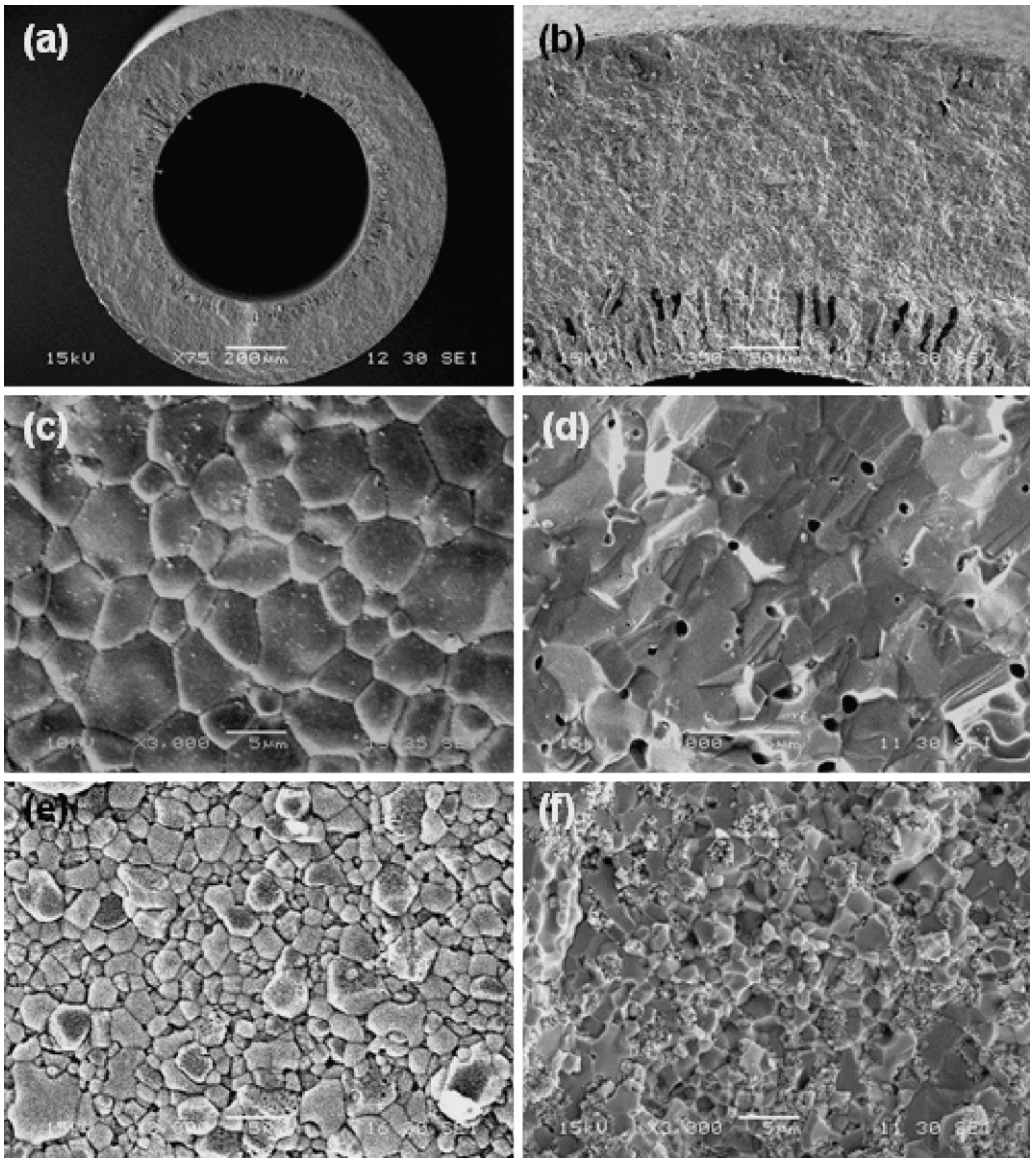

Fig. 7. SEM images of different skins of the HF4 co-sintered at 1500 °C; (a) overall view of the HF, (b) cross-section of the HF, (c) outer surface of the HF, (d) electrolyte cross-section of the HF, (e) inner surface of the HF and (f) anode cross-section of the HF.

with water vapour of 0.35 $cm^3\ min^{-1}$ using a bubbling cylinder at 20 °C, 1 atm) and air of 40 $cm^3\ min^{-1}$ (20 °C, 1 atm) were flowed through the anode and cathode, respectively, in a counter-flow arrangement. The *V–I* characterization was made using a potentiostat/galvanostat (Autolab® PGSTAT 30, Netherlands), at a current step of approximately 1.1 s.

Fig. 6 shows cell voltages and power densities as functions of current density for the dual-layer HF-SOFC at 450 °C, 550 °C and

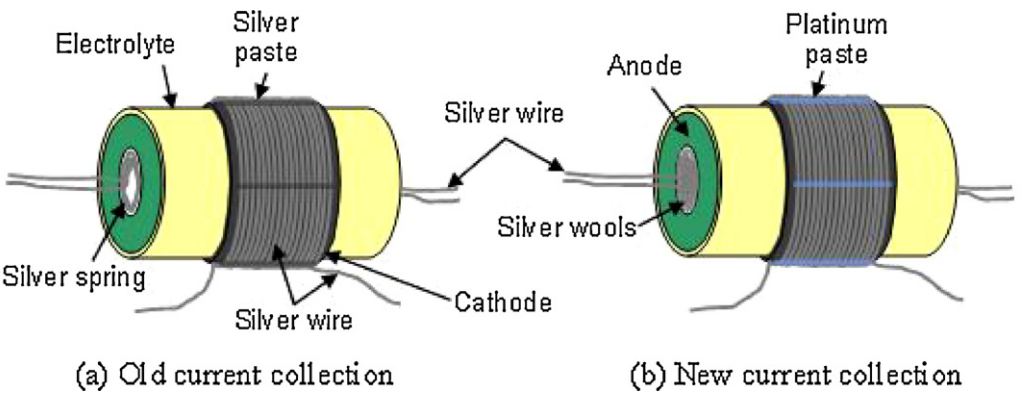

Fig. 8. Illustration of old and new current collections of the micro-tubular SOFC.

Table 4
Compositions of the spinning suspension and the co-extrusion conditions of HF5.

Experimental parameters	Values (electrolyte outer layer)	Values (anode inner layer)
Compositions of the spinning suspension (wt.%)		
NiO	0	42.00
CGO	64.00	28.00
PES	6.40	7.00
Arlacel P135	0.12	0.12
DMSO	29.48	22.88
Viscosity of the spinning suspension (cP)	3,930	31,400
Extrusion rate ($cm^3\ min^{-1}$)	0.5	7
Flow rate of internal coagulant ($cm^3\ min^{-1}$)	10	
Air gap (cm)	20	

580 °C. The open-circuit voltage (OCV) is measured as ca. 1.1, 0.9, and 0.8 V at 450 °C, 550 °C and 580 °C, respectively. This figure also shows experimental power densities as functions of current densities, in which the maximum power densities of 440 W m^{-2}, 800 W m^{-2} and 1000 W m^{-2} have been achieved at 450 °C, 550 °C and 580 °C, respectively, approximately one order of magnitude lower than those of micro-tubular SOFC prepared by Suzuki et al. [11] using conventional ram extrusion and sintering method. This can be attributed to (i) low porosities and TPB densities at the anode of the dual-layer HF prepared in this work, due to high co-sintering temperature (1550 °C) and (ii) poor cathode layer due to low sintering temperature (970 °C), and insufficient current collection from the inner fibre (anode) wall. Therefore, three approaches have been carried out in order to enhance the performance of the dual-layer HF, which is discussed in the following section.

3.3. Reduction of co-sintering temperature and improvement of cathode layer and current collection

As an attempt to increase the porosity of the anode, the co-sintering temperature of the dual-layer HF was reduced from 1550 °C to 1500 °C. As can be seen in Fig. 7, the porosities of the outer and inner layers are slightly increased with the decrease of co-sintering temperature. The CGO grain size is also become smaller, approximately from 9.6 μm to 5.9 μm, when the co-sintering temperature is reduced from 1550 °C to 1500 °C.

In order to produce a better cathode layer, the sintering temperature of the cathode was increased to 1200 °C for 5 h. For the enhancement of the quality of the current collection from the inner wall of the fibre, silver wool was used to replace the silver spiral wire. Silver wool was packed inside the fibre lumen to collect the anode current, producing excellent electrical contact with the anode wall, as illustrated in Fig. 8. The high porosity of the wool ensures fuel distribution to anode/electrolyte/gas triple-phase boundary (TPB) is not hindered significantly. The platinum paste was also used to replace silver paste as an effort to provide a better connection between the silver wire and the cathode surface.

The electrochemical performance of the improved fuel cell is shown in Fig. 9, in which the cell produced the maximum power densities 3400–6800 W m^{-2} at 550–600 °C, respectively. These maximum power densities are almost five times greater than the previous fuel cell, due to: (a) the increase of anode porosity, which achieved by co-sintering the dual-layer fibre at a lower temperature, has improved the hydrogen transport to, and reaction rates at, TPB; (b) better LSCF-CGO cathode layer, which were sintered at higher temperatures to increase cathode electrical conductivities; and (c) better electrical contact to the anode wall has decreased contact potential losses. However, the maximum power density is still ca. 40% lower than reported for similar micro-tubular fuel cells [11], largely due to the electrolyte layer thickness of ca. 10 μm, rather than ca. 80 μm in this work. Hence, further optimization of the CGO electrolyte layer thickness would minimise ohmic losses and increase power densities significantly.

3.4. Reduction in electrolyte thickness of dual-layer HF

Besides lowering co-sintering temperature for higher effective porosity of the anode layer and significant improvements to the cathode layer and current collection, another efficient way to further improve the performance of the fuel cell is by reducing thickness of the electrolyte layer. In this work, the extrusion rate of the electrolyte layer suspension has been reduced to 0.5 $cm^3\ min^{-1}$ in order to obtain thin electrolyte thickness. The compositions of spinning suspension and co-extrusion conditions that used for fabricating a new batch of fibre, which are named as HF5, are given in Table 4.

Fig. 10 shows the SEM images of the HF5 co-sintered at 1500 °C for 12 h followed by a reduction at 550 °C for 2.5 h. As the co-extrusion parameters for the inner layer were kept same as the previous fibre HF4, the anode structure of the HF5 is similar, consists short finger-like voids originating from the inner surface (approximately 35% thickness) with the rest of the anode occupies by a sponge-like structure. Much thinner outer electrolyte thickness of the dual-layer HF is achieved by simply reducing the corresponding extrusion rate, without affecting the structure of the anode inner layer. Viscosity of the spinning suspension for the outer layer should not be too high in order to ensure a smooth flow of the suspension and a full and uniform coverage, especially when the extrusion rate is very low. Therefore, the ceramic loading was reduced from 64 wt.% in the previous batch of fibre to 60 wt.%, as an effort to reduce the viscosity of the suspension. As can be seen

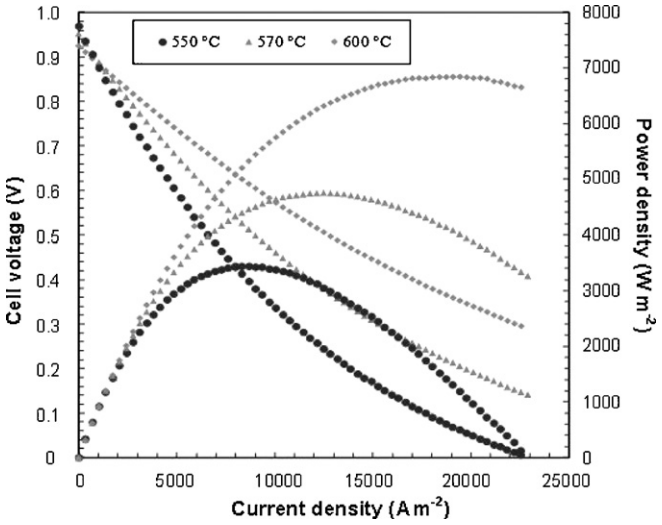

Fig. 9. Voltages and power densities as functions of current density of the improved cell HF4.

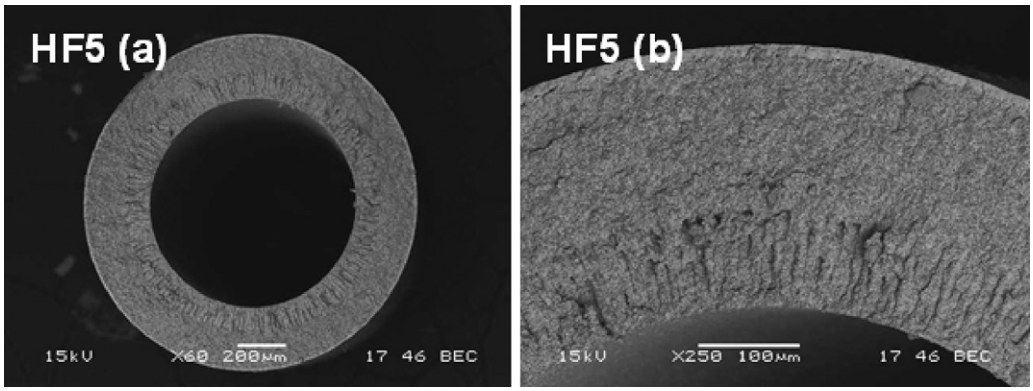

Fig. 10. SEM images of the (a) overall view and (b) cross-section of the CGO/Ni–CGO dual-layer HF of HF5.

in Fig. 10, dual-layer HF with 10 μm electrolyte thickness is successfully produced when the extrusion rate of the outer layer was reduced to 0.5 $cm^3\ min^{-1}$. It can also be observed that the thickness of electrolyte outer layer is very uniform deposited on the anode inner layer and covers the whole length of HF surface, and thus, shows another advantage of co-extrusion as a deposition technique of a thin layer on the HF support.

Fig. 11 shows cell voltages and power densities as a function of current density for the fuel cell prepared from fibre HF5 at operation temperatures of 550–600 °C. The maximum power densities achieved are 5,660 W m^{-2}, 7740 W m^{-2} and 11,100 W m^{-2} at temperature of 550 °C, 570 °C and 600 °C, respectively, which shows a significant improvement compared to the previous batch of cell. In thinner electrolyte, the oxygen ion from the cathode side could transport faster to the anode side and this would accelerate the kinetics and reactions in both electrodes. These results justify the need of reducing the electrolyte thickness due to the significant impact on the performance of the cell. In comparison with previous study, the maximum power density obtained for fibre HF5 at 600 °C, i.e. 11,100 W m^{-2}, is slightly lower than the one produced by conventional ram extrusion method with similar electrolyte thickness (10 μm) and at the same operating temperature [11], which was reported to be 12,900 W m^{-2}. Such lower value can be explained by the less effective porosity in the anode layer due to relatively short finger-like voids structure (~35%). Therefore, an optimization of the anode structure is required in further improving the performance of the dual-layer HF.

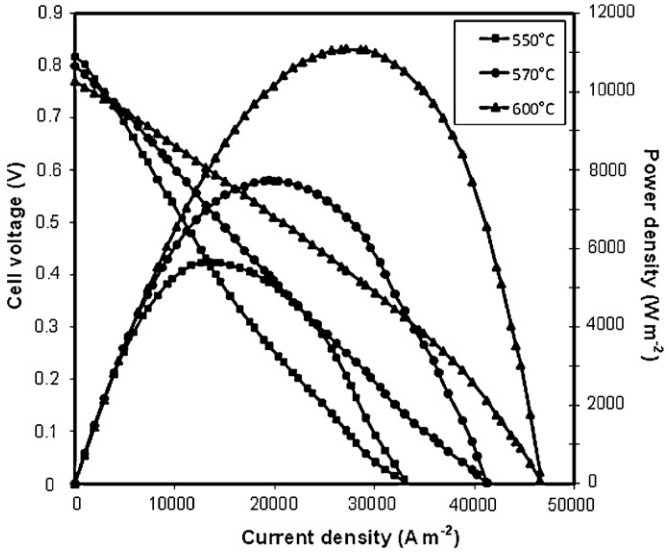

Fig. 11. Voltages and power densities as functions of current density for the cell of HF5.

4. Conclusions

Four CGO/NiO-CGO dual-layer hollow fibre (HF) precursors with different anode structures, i.e. HF1, HF2, HF3 and HF4, were successfully developed in the early stage of this study by controlling the viscosity of the spinning suspension. Only HF4, which consists 35% finger-like voids structure from the anode inner surface, was co-sintered at 1550 °C for 12 h and then reduced using hydrogen to form CGO/Ni-CGO HF, prior to the preparation of the fuel cell from this HF. The electrochemical performance was carried out and the cell produces the maximum power densities of 440–1000 W m^{-2} at 450–580 °C. Due to the low power output compared to the micro-tubular SOFCs prepared by other research groups, three improvements on the fuel cell, i.e. (i) reducing the co-sintering temperature from 1550 °C to 1500 °C, (ii) producing better cathode layer and (iii) improving current collection from inner (anode) wall, have been carried out and the maximum power densities of the cell achieved is about five times higher than that of the first batch of cell. Another efficient way to further improve the performance was done in this study by reducing the thickness of the electrolyte layer, which this new HF is named as HF5. With the decrease in the extrusion rate of the outer layer suspension to as low as 0.5 $cm^3\ min^{-1}$, the electrolyte thickness of 10 μm can be produced. From the result obtained, the cell with the electrolyte layer of 10 μm shows the highest performance among those cells that fabricated previously, which reaches up to 11,100 W m^{-2} at 600 °C.

Acknowledgements

The authors gratefully acknowledge the research funding provided by EPSRC (EP/E00136X) in the United Kingdom. The award of an overseas study bursary to MHDO by the Malaysian Ministry of Higher Education (*MoHE*) and Universiti Teknologi Malaysia (*UTM*) is also gratefully acknowledged.

References

[1] K. Kendall, N.Q. Minh, S.C. Singhal, in: C.S. Subhash, K. Kevin (Eds.), High Temperature and Solid Oxide Fuel Cells, Elsevier Science, Amsterdam, 2003, pp. 197–228.
[2] T. Suzuki, T. Yamaguchi, Y. Fujishiro, M. Awano, Journal of Power Sources 160 (2006) 73–77.
[3] N. Droushiotis, M.H.D. Othman, U. Doraswami, Z. Wu, G. Kelsall, K. Li, Electrochemistry Communications 11 (2009) 1799–1802.
[4] M.H.D. Othman, Z. Wu, N. Droushiotis, U. Doraswami, G. Kelsall, K. Li, Journal of Membrane Science 351 (2010) 196–204.

[5] N. Droushiotis, U. Doraswami, D. Ivey, M.H.D. Othman, K. Li, G. Kelsall, Electrochemistry Communications 12 (2010) 792–795.
[6] M.H.D. Othman, N. Droushiotis, Z. Wu, K. Kanawka, G. Kelsall, K. Li, Journal of Membrane Science 365 (2010) 382–388.
[7] X. Tan, S. Liu, K. Li, Journal of Membrane Science 188 (2001) 87–95.
[8] B.F.K. Kingsbury, K. Li, Journal of Membrane Science 328 (2009) 134–140.
[9] J.H. Kim, B.R. Min, J. Won, H.C. Park, Y.S. Kang, Journal of Membrane Science 187 (2001) 47–55.
[10] J.C. Chen, C.L. Chang, C.S. Hsu, B.H. Hwang, Materials Research Bulletin 42 (2007) 1674–1682.
[11] T. Suzuki, Y. Funahashi, T. Yamaguchi, Y. Fujishiro, M. Awano, in: T.S. Zhao (Ed.), Micro Fuel Cells, Academic Press, Boston, 2009, pp. 141–177.